Stability, Structure and Reconstruction of 1H-Edges in MoS 2

Yuman Sayed-Ahmad-Baraza, Christopher Ewels

FULL PAPER

Stability, structure and reconstruction of 1H-edges in MoS_2

Yuman Sayed-Ahmad-Baraza,[a] and Christopher P. Ewels*[a]

Abstract: We present density functional studies of the edges of single-layer 1H-MoS_2. This phase presents a rich variability of edges that can influence the morphology and properties of MoS_2 nano-objects, play an important role in industrial chemical processes, and find future applications in energy storage, electronics and spintronics. For so-called Mo-100%S edges we confirm vertical S-dimers are stable, however we also identify a family of metastable edges combining Mo atoms linked by two-electron donor symmetrical disulfide ligands and four-electron donor unsymmetrical disulfide ligands. These may be entropically favoured, potentially stabilizing them at high temperatures as a "liquid edge" phase. For Mo-50%S edges, S-bridge structures with 3× periodicity along the edge are the most stable, compatible with a Peierls' distortion arising from the d-bands of the edge Mo atoms. We propose an additional explanation for this periodicity via the formation of 3-centre bonds.

Introduction

Many different types of edge exist for MoS_2, each with a different atomic configuration. When reducing the lateral size of the 2D sheets to the nanoscale the properties of the edges become important and the relative stability of the different edges controls the morphology of small nanoclusters of MoS_2. Edges play a crucial role in catalytic processes,[1,2] such as the hydrodesulfurization reaction,[3–5] the hydrogen evolution reaction,[2,6,7] and the chemical functionalization of MoS_2 [8,9]. They are also suggested to be important as anode catalysts in solid oxide fuel cells,[10] and to have possible application as high power, fast charge/discharge cathodes for Li-ion batteries,[11] and spin-filters [12]. It is, therefore, important to understand the atomic structure and stability of the edges, and to consider their role in the functionalization of MoS_2 nanosheets.

Edge morphology depends on factors such as synthesis conditions [3,13–15] and particle size [16]. Different edge morphologies present different properties, for example metallic character and magnetism have been predicted for specific edges. [16,17] Two types of edges are normally considered according to the direction along which the MoS_2 sheet is cut: armchair and zigzag (Figure 1a). Although the (1$\underline{2}$1$\underline{0}$) armchair edge [18] is unique, there are two (10$\underline{1}$0) zigzag edges: the Mo- and S-edges [17]. The truncated S-edge in Figure 1a is completely saturated (S-100%S) while the Mo-edge is non-saturated (Mo-0%S). Other degrees of S saturation are indicated in a similar way (Figure 1b).

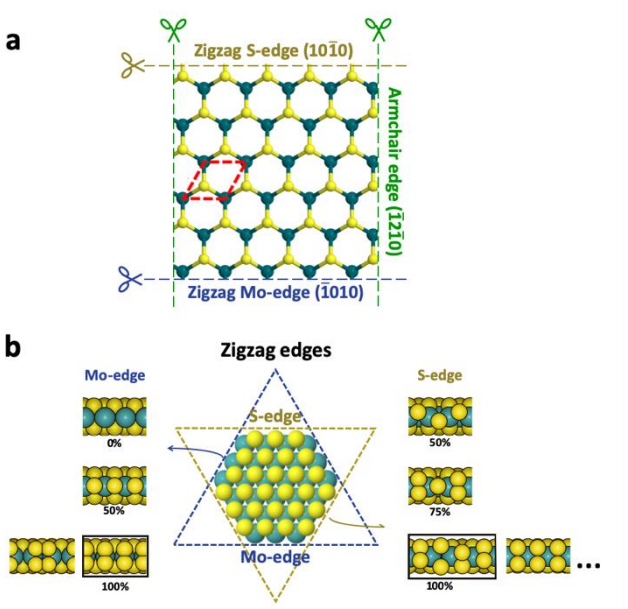

Figure 1. a) *Classification of MoS_2 edges. b) Geometric link between the type of exposed zigzag edge and the flake shape. These edges can have different degrees of S saturation, shown schematically. Most stable edges are marked with a black box. The edge configurations in panel b are schematic illustrations based on the structures calculated in* [17,19–21]

Previous studies found the most thermodynamically stable edges are the 50%S and 100%S Mo- zigzag edges for a wide range of experimental conditions.[5,13,14,19,22–24] While many metastable structures have been predicted for the S-100%S edge,[5,19,21,25] only two have been proposed for the Mo-100%S edge [12,17,19,26]. As well as a structure with vertical S-dimers at the edge, another less stable configuration with horizontal S-dimers has also been proposed [17]. Here we explore other possibilities.

Mo-50%S edges form by S atoms bridging neighbouring Mo atoms. Previous studies show that periodic lattice distortions occur along these edges. [12,17,19,21,27] In the current study we explore different possible distortions on this edge and determine the most favourable. Finally, we propose a qualitative model for understanding the mechanism behind the distortion.

Results and Discussion

We refer hereafter to the ribbon models as *L*x*W*, with *L* the length of the unit cell in the direction parallel to the edge in terms of the number of edge Mo atoms; and *W* the width of the ribbon in terms of the number of Mo rows parallel to the edges (including the edges). When comparing the stability of different structures, it is useful to normalise the values with respect to a common edge unit.

[a] Dr Yuman Sayed-Ahmad-Baraza, Dr Christopher Ewels
Institut des Matériaux Jean Rouxel, CNRS UMR6502, Université de Nantes, 2 Rue de la Houssinière, BP32229, 44322 Nantes, France.
E-mail: chris.ewels@cnrs-imn.fr

Supporting information for this article is given via a link at the end of the document.

We choose this unit to be the primitive unit cell of the corresponding ribbon presenting the structure of the truncated single-layer (shaded rectangle in Figure 2). This corresponds to normalising the energies to a ribbon of 1x*W*. We will call this common unit a "fundamental edge unit" (f.e.u.).

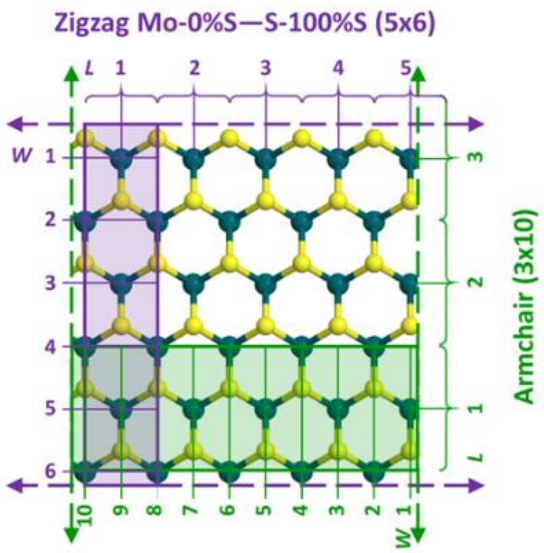

Figure 2. Nomenclature for *LxW* ribbon models. Shaded boxes give examples of a 1x6 Zigzag (purple) and 1x10 Armchair (green) ribbon, corresponding to the "fundamental edge unit" (f.e.u.) in each direction. The purple Zigzag ribbon extends infinitely from left to right, the green Armchair ribbon from top to bottom.

1. The Mo-100%S Edge

We first examine the Mo-100%S edge. To date, vertical dimer (VD) and opposed horizontal-dimer (HD-O) S-dimer configurations have been explored,[17] but others can be imagined (see Figure 3). Notably, rotating vertical edge S-dimers in an alternate manner gives an edge where half of S atoms lie in Mo-50%S-like positions while the other half remain in Mo-100%S-like positions (R*x* in Figure 3). We have explored two initial configurations: one starting with vertical S-dimers and a second where the vertical S-dimers are broken (R1 and R2 in Figure 3)
After geometrical optimisation (starting with slightly distorted configurations in order to break the symmetry), the relaxed structures are presented in Figure 4. HD-O is 0.31 eV per f.e.u. less stable than VD structure, in relatively good agreement with 0.25 eV from the literature [17]. The staggered horizontal dimers (HD-S) are not stable and evolved to a very different structure 0.44 eV per f.e.u. less stable than the VD.

The relaxed HD-S structure alternates between two staggered horizontal S-dimers and two tilted staggered S-dimers. Neither R1 nor R2 are stable, evolving into structures similar to the one found for HD-S with comparable energy, but consisting of only tilted staggered S-dimers.

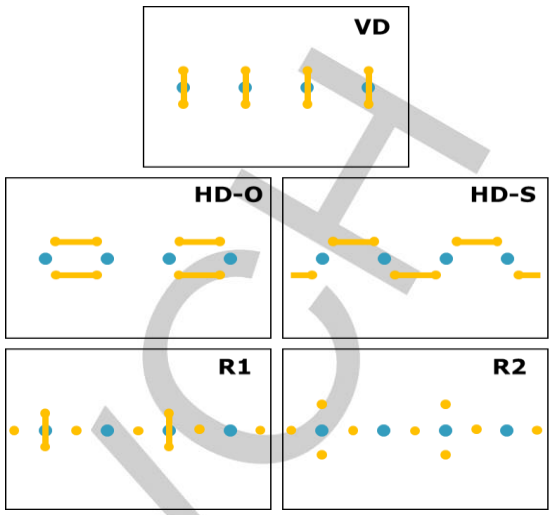

Figure 3. Schematic of the Mo-100%S edge configurations (side view) in this study: vertical S-dimers (VD), horizontal dimers in an opposite (HD-O) or staggered (HD-S) fashion. Rotating half of the vertical dimers in VD (R1), and with S-S bonds broken (R2). Blue and yellow circles represent edge Mo and S atoms respectively, S-dimers indicated by a yellow line.

Interestingly all three cases are composed of tilted staggered S-dimers, a repeating pattern with one S atom close to that of the Mo-50%S edge. If we take this repeating pattern as a design unit (Figure 5a), many possible structures can be formed from it. Representing the repeating pattern as an arrow, this arrow can orient in four ways along the edge (Figure 5b). Our supercell contains two repeat patterns, which if arranged independently give four non-equivalent combinations (Figure 5c-f). More combinations can be obtained using bigger supercells (e.g. Figure 5g). The R1 and R2 structures correspond to the two possible structures presenting head-tail interactions (Figure 5c and d). A third structure (R3) shown in Figure 5e is only 0.39 eV higher in energy than VD and thus the most stable among the new configurations presented here (HD-S, R1, R2 and R3). Nevertheless, due to the small differences between these four values we should regard this qualitative energy order with caution. The remaining possibility with head-head and tail-tail interactions has not been calculated (Figure 5f), because it contains two S atoms that would be too close to each other and hence unstable. The most stable configuration VD is consistent with the previous experimental studies found in the literature. Nevertheless, knowing the structure and relative energies of other metastable configurations is important to understand chemical processes occurring at the edges. Furthermore, for structures combining unsymmetrical and symmetrical disulfide bonds (those represented in this study by combinations of arrows) we need to take entropy into account. As each structure, can be represented as a combination of a repeating pattern that can be arranged in four different ways, the number of possible combinations grows rapidly when considering longer edges. Thus the entropy associated with this collection of structures is higher than for the stable VD structure and these structures could be stabilised with respect to VD at high temperatures.

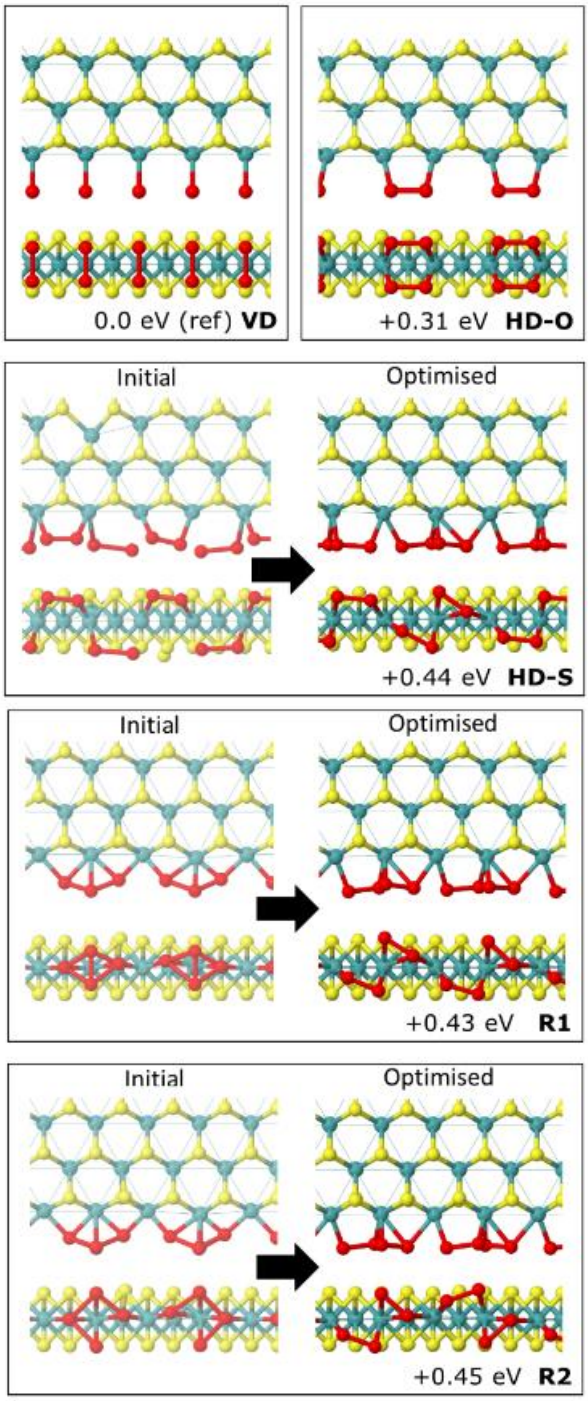

Figure 4. *Top and side views of the optimised edge structures calculated in this study. For HD-S, R1 and R2 the initial geometry considered for the optimisation is also represented (slightly faded to white). The relative energy per f.e.u. of each structure with respect to VD, the most stable edge structure, is indicated. Atom colour code: blue-green (Mo), yellow (S), red (edge S).*

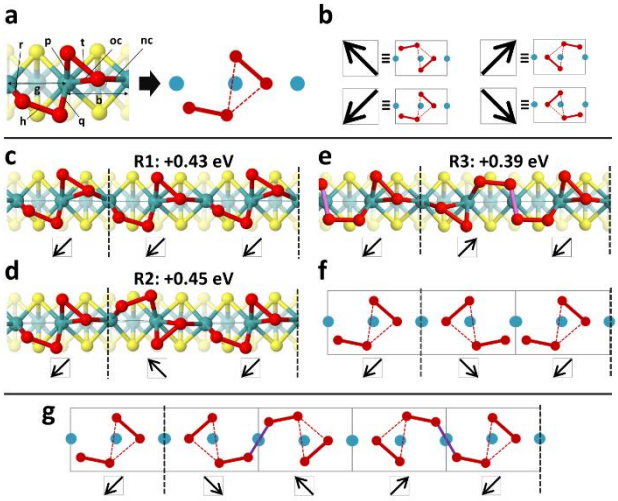

Figure 5. *a) Atomic structure of the repeating S-edge pattern and its schematic representation. b) Arrow representation of the repeating pattern and its four possible arrangements. c-f) The four possible non-equivalent combinations of the repeating pattern for a L=4 supercell (2 repeating patterns). The relative energy per f.e.u. of each structure with respect to VD is indicated. g) Additional structure possible in a doubled unit cell. Atoms coloured: blue-green (Mo), yellow (S), red (edge S). Basal atoms are faded white. (e,g) A possible new S-S bond shown in violet.*

Images of the six calculated structures (VD, HD-O, HD-S, R1, R2 and R3) with bond lengths are given in Supplementary Figures S1-S6. For VD we obtained a Mo-S distance of 2.41 Å at the edge, and S-S distance for the S-dimers of 2.00 Å. Comparing the Mo-Mo distance from edge to second row Mo atoms (3.02 Å) with the bulk (3.13 Å) shows that the edge retracts inwards. The structure is symmetric without any observed coupling of the S-dimers and a constant distance of 3.13 Å between Mo atoms along the edge. For the HD-O structure the edge Mo-S and S-S distances are longer at 2.46 Å and 2.02 Å respectively. The edge also retracts inwards and in this case the Mo-Mo distances along the edge are affected by the horizontal S-dimers, with shorter distances where the S-dimers are formed (2.93 Å) alternated by longer Mo-Mo distances (3.32 Å). These results are in agreement with previous literature. [17]

We now consider the geometry of the new structures found (HD-O, R1, R2 and R3). In some cases, the bridging S atom adopts a more symmetric position with nearly equal Mo-S bonds (~2.5 Å) and closer to the plane of Mo atoms (R1, R2 and R3), while in other cases less symmetric bridges form with unequal Mo-S bonds (~2.7 Å and ~2.4 Å) and more deviation from the plane of the Mo atoms (HD-S, R1 and R3). In general, the bridging S atom forms shorter bonds with the Mo atom that has a lower coordination (with the exception of the more symmetric bridge of R1). The bridging angle (Mo-S-Mo) varies from 73.0° and 83.5° depending on each specific bridge. The more symmetric bridges are associated with longer Mo-Mo distances and higher angles. In general Mo-S distances at the edge tend to be longer than in the bulk (2.39 Å), with the exception of some shorter bonds in R1

and R2. The S-S bonds at the edge are similar in all cases (2.01-2.07 Å), similar or marginally longer than the horizontal pairs of HD-O (2.02 Å). In the case of the R3 structure a potential vertical S-S bond could arise from the "head-head interaction", marked in violet in Figure 5e and g, although longer (2.38 Å) than the vertical (VD) or horizontal S-dimers.

Mo-Mo distances vary depending on whether they are bridged by a S atom ("b" in Figure 5a, longer than bulk), or not, for which there is a gap ("g" in Figure 5a, at ~3.0 Å smaller than bulk 3.13 Å). The Mo atoms are also displaced along the other directions. First, it can be observed in the side view of R2 that Mo atoms are slightly displaced over and under the average plane of Mo atoms, producing a wave pattern. Finally, Mo atoms are also displaced along the in-plane direction perpendicular to the edge, creating a soft wave pattern visible in the top views of HD-S and R3. Edge effects on the geometry decay rapidly moving inwards, reaching bulk bond lengths by the third row back.

The bridging S atoms have been represented with one bond with each of their two Mo neighbours. As these S bridging atoms are presenting three bonds in total, is it correct to represent both S-Mo interactions as a covalent bond? This question is even more relevant for the less symmetrical bridges, where one Mo-S distance is clearly shorter than the other.

The chemistry of polynuclear complexes containing S ligands is very rich.[28,29] This type of S-bridge has been predicted [30] and experimentally observed [31–36] in metal complexes. $[(CH_3)_5C_5MoS_5]_2$ [31] and $[Mo_4(NO)_4S_{13}]^{4-}$ [32] are good examples containing S-bridging ligands similar to those found here for MoS_2 edges. A disulfide ligand can connect two metallic centres in four different ways (Figure 6a),[30] in three categories according to how many electrons they contribute to the interaction with the metallic centres. In the two-electron donor case the disulfide ligand forms one formal bond with each metallic centre, leaving four lone-pair electrons available for coordination with the metallic centres. Donation of one or two of these lone-pairs transforms the ligand in a four-electron or six-electron donor respectively. Since these are dative bonds the number of formal covalent bonds and the oxidation state of the metallic centres remain constant in all cases. Counting the number of electrons that the disulfide ligand donates is useful in the context of the 18-electron rule, the equivalent of the octet rule for metals.[37] As examples, in the case of the complex $[(CH_3)_5C_5MoS_5]_2$ [31], considering the "unsymmetrical disulfide" ligands as four-electron donors gives to the metallic centres the favoured 18-electron configuration.

Following this classification, the disulfide ligands at the MoS_2 edges can be understood as a combination of two-electron donor ("symmetrical disulfide") and four-electron donor ("Unsymmetrical disulfide") ligands. The repeating unit in Figure 5a is composed of a "head" two-electron donor disulfide, and a "tail" four-electron donor disulfide, in our arrow representation. Thus, for the bridging S atom, the shortest bond is covalent and the longest is dative. More symmetric bridges contain two resonance structures that alternate the dative bond between both Mo-S bonds. It is interesting to note that the six-electron donor ("bridging disulfide") in Figure 5 is consistent with the predicted vertical S-pairs formed in the S-100%S edge (Figure 1b).

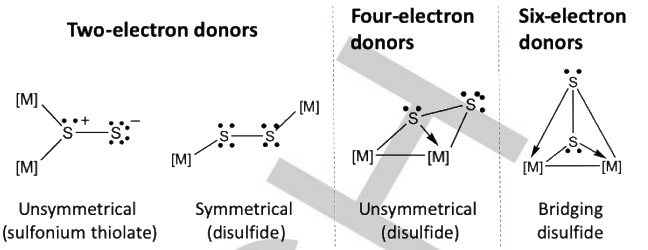

Figure 6 *Different bonding modes of a bridging disulfide ligand classified according to how many electrons of the ligand are implicated in bonding with the metallic centre [M] (using the neutral formalism for electron counting), following classification and nomenclature from* [30].

We next analyse how many electrons we can assign to the edge Mo atoms. The S ligands in the bulk are bridging three Mo atoms, and are considered as four-electron donors (two unpaired electrons and one lone-pair).[28] As the three bonds are equivalent, from a valence-bond description point of view, the bonding is described using three resonance structures alternating the dative bond over the three bonds. In this way we can consider that each S atom is using four electrons for three bonds, and thus, allowing fractional number of electrons in the counting scheme, they contribute with 4/3 electrons to each Mo atom. As each edge Mo atom is connected to four internal S atoms, the internal contribution to each edge Mo atom is thus $4\times(4/3)\approx5.33$ electrons. Depending on the structure, the edge S neighbors contribute from 8 to 10 electrons, giving a total electron count on edge Mo atoms from 13.33 to 15.33. While this is deficient in terms of the 18-electron rule it straddles the bulk MoS_2 value of 14. With a molecular orbital approach we obtain six bonding and one non-bonding levels for bulk MoS_2 or in a general trigonal prismatic complex model.[38,39] This means that filling the molecular orbitals with 14 electrons, we completely fill all bonding/non-bonding levels leaving empty the antibonding levels. Nevertheless, if we want associate these electron counts at the edges with stabilising or destabilising situations a rigorous analysis considering the specific coordination symmetry of the edge Mo atoms should be done.

2. The Mo-50%S Edge

The Mo-50%S edge is formed by S atoms bridging edge Mo atoms (Figure 7). DFT calculations have predicted that symmetric Mo-Mo and Mo-S lengths along the edge are not stable. [17]

Calculations using bigger supercells have found structural distortion. While most have focused on 2× periodic superstructures, 3× [21] and 4× [27] structures have recently been proposed. The distortions consist of variable Mo-Mo lengths along the edge, and in-plane S- displacements orthogonal to the edge ('*out-*' or '*in-*' S-bridges). Although it is known that the 2× edge is ~40 meV [17] per f.e.u. more stable than the undistorted, the relative stability of the 3× and 4× structures remains unknown. In addition, other structures combining '*in-*' and '*out-*' S-bridges are possible for 3× and 4× (and greater) periodicities besides those proposed in previous literature.

To address these questions, we have simulated structures with 1× to 4× periodicities, with a frozen S-0%S edge on the opposite side of the ribbon. We have started optimization from multiple configurations. For the 2× case, a '1*out*-1*in*' configuration, and a "pairwise" configuration where edge-S atoms are pushed towards each other in pairs, for the 3× case a '2*out*-1*in*' and '1*out*-2*in*' structures, and for the 4× case a '3*out*-1*in*', '1*out*-3*in*', and the two possible '2*out*-2*in*' cases, '*out-out-in-in*' ("consecutive") and '*out-in-out-in*' ("alternated"). After optimization, for each periodicity only a single minimum energy structure was found.

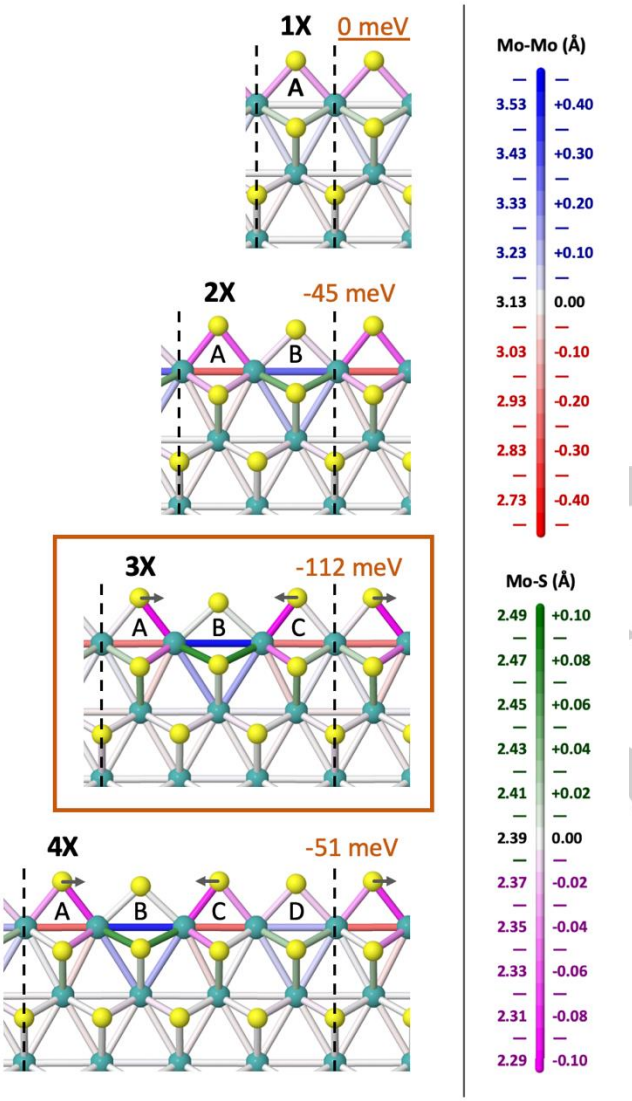

Figure 7. *Mo-50%S edges for different supercell widths (L= 1- 4), indicated by dashed lines. Red (magenta) and blue (green) bonds represent compressed and elongated Mo-Mo (Mo-S) bonds with respect to the infinite single-layer (white). Values at the left (right) of the colour key bars represent absolute (relative to infinite single-layer) bond distances. Arrows indicate direction when S-atoms shift along the ribbon length. Relative energy per f.e.u. with respect to the 1× model is indicated, 3× is the most stable periodicity.*

The optimised structures with their relative energies are shown in Figure 7, with structural parameters in Supplementary Table S1. While for the 1× cell symmetry is imposed, for the 2× cell symmetry breaks, with alternating '*in*-' and '*out*-' S bridges. This relaxation stabilizes the edge by 45meV per f.e.u (or edge S atom), in very good agreement with the value obtained by Lucking *et al* (~40 meV) [21]. In the case of the 4× periodicity, the 2*out*-2*in* "alternated" structure is stable with two non-equivalent *in* S-bridges, one with a more elongated Mo-Mo distance, slightly different to previous literature [27]. However this extra symmetry breaking over the 2× case only lowers the edge energy by a further 6meV/f.e.u.. Instead, the most stable relaxation is for 3× periodicity where one S atom displaces inwards and two outwards (1*in*-2*out*), matching the structures found in the literature for this periodicity [21,27]. The outward displaced S atoms also displace along the ribbon axis towards the inward displaced S-atom, producing a structure with C_{2v} symmetry with mirror planes and C_2 axes located bisecting the '*in*-' bridge and between the '*out*-' bridge. In this case symmetry lowering stabilizes the structure by 112meV per f.e.u. over the 1x cell.

To verify the importance of the opposing edge structure of the ribbon, we performed some calculations considering a S-50%S opposite edge for the same periodicities. This preserves the stoichiometry of the infinite single-layer and saturates Mo dangling bonds on the opposing ribbon edge. Structures, energies and structural parameters are given in Supplementary Figure S7 and Supplementary Table S1. Although there are some minor variations in bond lengths and absolute energies, the overall structures obtained remained unchanged, along with their relative energy ordering, giving us confidence in the results presented above.

Lucking *et al*. developed an electron counting model to justify the 3× edge periodicity.[21] In order to test this we calculated the atomic Mulliken charges of the 3× structure, finding a charge of +0.54 for the Mo atoms in the ribbon centre which have a formal oxidation state of +4. The edge Mo atoms were very slightly less charged, with charges of +0.48 and +0.49 for the Mo atoms that were assigned +4 and +5 oxidation states by Lucking *et al*. The fact that these two edge Mo atoms have nearly equal charges casts doubt on the multivalency picture.

We can count the electrons in the Mo centres using the same model used earlier to discuss Mo-100%S edges. We assume that each internal S atom pulls 2/3 electrons from each Mo atom, and each edge S-bridge pulls 1 electron from each Mo neighbour, in order to reach its oxidation state of -2. Allowing fractional oxidation states, this results in a partial oxidation state of +4.67 on each edge Mo atom. This implies that each edge Mo has 1.33 valence electrons, compatible with 1 electron per metallic centre and another electron shared by the three centres. If we localise this shared electron in one of the Mo atoms we arrive to the multivalency situation proposed by Lucking *et al*, with one Mo atom with two valence electrons and two Mo atoms with one valence electron.

The coordination around the edge Mo atoms in the undistorted 1x structure presents C_{2v} symmetry (Figure 8a), splitting the atomic d-orbitals giving five singly degenerate levels. The multivalency situation proposed by Lucking *et al*. would involve one Mo atom

with its lowest level completely filled, and two Mo atoms with its lowest level half-filled giving one Mo-Mo bond. This does not match the '2*out*-1*in*' configuration obtained, with two Mo-Mo bonds per unit cell. An alternative is 1 electron per Mo atom and 1 electron shared by the three Mo atoms. In this situation each Mo atom would have its lowest level with a filling of 2/3, and the structure could suffer a Peierls' distortion with 3× periodicity. We now discuss this possibility in more detail.

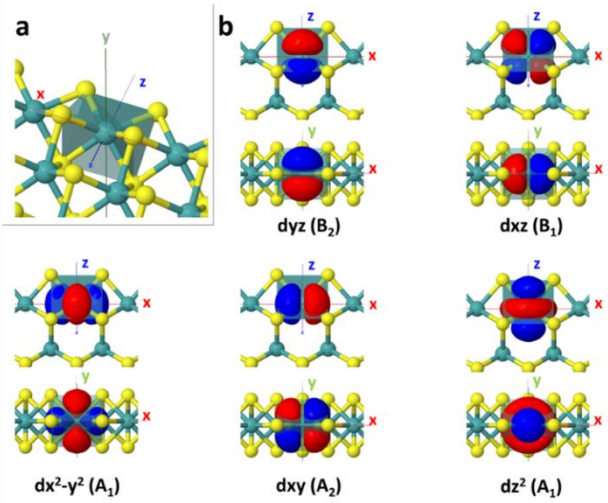

Figure 8. *a) Polyhedron with C_{2v} symmetry defining the coordination of S atoms around the edge Mo atoms in an undistorted Mo-50%S edge b) Top (y) and side (z) views of splitting of singly degenerate atomic d-orbitals in this C_{2v} crystal field. Symmetry type is given in parenthesis. Orbitals shown are illustrative and not the result of a calculation*.

Examining the shape and directionality of the schematic d-orbitals in Figure 8b, many of them can interact with neighbouring edge Mo-atoms. For example, A_1-orbitals from neighbouring Mo atoms can form σ bonds, while the A_2-orbitals could form π bonds. Formation of three-centre orbitals will result in two electrons filling the most stable bonding molecular orbital, while the remaining 2 electrons may fill a non-bonding molecular orbital (leading to a 3-centre 4-electron bond) or another bonding three-centre molecular orbital (leading to two 3-centre 2-electron bonds). This would be preferred over the situation previously proposed with one filled two-centre bonding orbital and one filled non-interacting d-orbital. This type of analysis combining Peierls-like distortions arguments and local bonding rules has been traditionally used for the qualitative interpretation of bulk periodic lattice distortions in transition metal dichalcogenides with relatively good success [40–42].

Literature wave-functions plots of the metallic band of the 2× Mo-50%S edge [12,17] are indeed compatible with σ -bonding of A_1 (dx^2-y^2) orbitals between neighbouring edge Mo atoms. Of all the d-orbitals in Figure 8b this can best interact along the edge, and should be the lowest energy level after C_{2v} field splitting (as it has less overlap with the S ligands). Thus, the Peierls' distortion (or alternatively the 3-centre 4-electron bond) likely involves this orbital.

Therefore, we propose that the preference for the 3× periodic Mo-50%S-edge structure may be a consequence of a Peierls' distortion. In addition, the preference of the 2out-1in structure is likely related with the formation of three-centre bonds, without the need to invoke a multivalency description. This is consistent with the fact that the Mulliken charges for both type of edge Mo atoms are similar. Nevertheless, it does not explain why edge Mo atoms appear less charged than the internal Mo atoms, as we would expect the opposite taking into account the electron counting model used in this discussion. In addition, if the different interacting d-levels are close in energy, their bands could overlap or mix, and the filling of the bands would differ from the proposed 2/3. In any case, the model presented here is qualitative, and further studies on the electronic structure of the different distorted structures would be needed in order to fully explain the mechanism behind the distortions.

Conclusions

The edges of 1H-MoS_2 present a very rich chemistry and physics. For Mo-edges, previous calculations predict a vertical S-dimer (VD) structure for the Mo-100%S edge, and bridging edge-S atoms for the Mo-50%S edge. However other metastable configurations may play a role in functionalisation and catalytic processes.

For the Mo-100%S edge we confirm the VD stability, showing staggered horizontal S-dimers are not stable. However, we also find a large family of metastable structures combining edge Mo atoms with effective edge coordination numbers of 2 and 3 linked by two-electron donor symmetrical disulfide ligands and four-electron donors unsymmetrical disulfide ligands. Although less stable than either VDs or horizontal dimers, these metastable structures could appear as intermediate states during chemical processes. In addition, as the number of possible configurations is very high for long edges they will be entropically favoured, potentially stabilizing them at high temperatures as a "liquid edge" phase.

For the Mo-50%S edges, the S-bridge structures are dependent on the size of the unit cell. It was known that the undistorted structure with 1× edge periodicity was not stable, and structures with periodicities from 2× to 4× had been proposed, although the relative stabilities between them was unknown, and a complete study of all the possible structures compatible with these periodicities, had not been yet investigated.

We find that 3× periodicity is the most stable, consisting of two asymmetric S-bridges shifted outwards associated with short Mo-Mo distances, and one symmetric S-bridge shifted inwards associated with a long Mo-Mo distance. Previous studies had proposed a multivalency model for the edge Mo atoms in this structure using an electron counting models.[21] However, our Mulliken charge analysis indicates that all edge Mo atoms have practically the same partial charge, incompatible with this literature model. Instead, using a similar electron counting model we propose that the 3× periodicity is compatible with a Peierls' distortion arising from the d-bands of the edge Mo atoms. In addition, we have proposed an alternative model based on local

bonding approximations, which could explain the formation of the observed pattern with two short and one long Mo-Mo distances by the formation of 3-centre bonds.

Experimental Section

Density functional theory calculations were performed using the local density approximation (LDA) as implemented in the AIMPRO code [43–46] (discussion of the functional choice is given in [8]). The spin-averaged charge density is fitted to plane waves with an energy cut-off of 100 Ha, while Kohn-Sham wave functions were constructed using localised Cartesian Gaussian orbital functions (50 for Mo, $l \leq 3$, 28 for S, $l \leq 2$). Relativistic pseudopotentials generated by Hartwigsen, Goedecker and Hutter were used,[47] with a finite electron Fermi temperature of 0.04 eV. Absolute energies were converged to better than 10^{-5} Ha during the self-consistency cycle.

The "ribbon approach" is adopted for modelling the edges, using periodic boundary conditions in all 3 dimensions. Bulk single-layer MoS_2 was modelled using a hexagonal 8x8x1 supercell with a single k-point in Γ, giving an optimised lattice constant of a=25.02 Å. The lattice constant for the direction perpendicular to the sheet, kept frozen during the optimisation, is set to 31.08 Å in order to avoid interaction between the repeating sheets. This structure was used as template for designing the ribbons (Supplementary Figure S8). During optimisation of the ribbon models all lattice parameters were kept frozen.

Mo-100%S edges were modelled using a 4x8 ribbon in a triclinic cell with lattice parameter along the edge and angle between the in-plane lattice vectors (120°) chosen to match the continuous monolayer. The lattice parameters are a=63.50 Å, b=12.51 Å, c=31.08 Å, with a 1x2x1 k-point grid centred at Γ. The opposite edge is set as S-0%S in order to maintain the stoichiometry of the infinite sheet. The geometry of the 2 first rows of atoms (i.e. the first row of MoS_2 units) from this edge was set equal to that of the continuous monolayer, and their coordinates frozen during optimisation.

Mo-50%S edges were modelled using a ribbon width W=10. Different supercells were considered with L=1, 2, 3 and 4. An orthorhombic cell was used, with the ribbon parallel to one of the lattice vectors, with lattice parameters a=42.33 Å (orthogonal to the edge), b=3.13 Å, 6.25 Å, 9.38 Å and 12.51 Å (parallel to the edge) for L= 1, 2, 3 and 4 respectively and c=15.88 Å (orthogonal to ribbon plane). In this case we used a 1xNx1 k-point grid centred in Γ, with N=24, 12, 8 and 6 for the models with L=1, 2, 3 and 4 respectively. The SCF energy was converged to $<10^{-8}$ Ha and optimisation threshold for atomic force $<10^{-4}$ Ha/a_0. We tested both S-0%S and S-50%S edges on the opposite edge. During these optimisqtions the same row of MoS_2 units as in the case of the Mo-100%S on the opposite edge are frozen at infinite monolayer positions (Supplementary Figure S8). Symmetry was taken into account during the optimisation. A symmetry plane situated on the plane of Mo atoms was considered, which constrains the S atoms along the edges to the plane of Mo atoms in the Mo-50%S models.

These opposite edges are only auxiliary edges and do not represent the actual configuration of S-0%S and S-50%S edges. The purpose is to have a constant edge mimicking as much as possible the infinite sheet, so changes in the structure of this edge are not allowed and thus will not contribute to the energy differences of ribbons with different Mo-edges.

Acknowledgements

Calculations were performed at CCIPL, Université de Nantes. This project has received funding from the European Union's Horizon 2020 research and innovation program under the Marie Sklodowska-Curie Grant agreement No 642742.

Keywords: MoS_2, edges, DFT, calculations, structure ,1H-MoS_2

[1] T. F. Jaramillo, K. P. Jorgensen, J. Bonde, J. H. Nielsen, S. Horch, I. Chorkendorff, *Science* **2007**, *317*, 100–102.
[2] H. Wang, Q. Zhang, H. Yao, Z. Liang, H.-W. Lee, P.-C. Hsu, G. Zheng, Y. Cui, *Nano Lett.* **2014**, *14*, 7138–7144.
[3] J. V. Lauritsen, M. Nyberg, J. K. Nørskov, B. S. Clausen, H. Topsøe, E. Lægsgaard, F. Besenbacher, *J. Catal.* **2004**, *224*, 94–106.
[4] G. A. Camacho-Bragado, J. L. Elechiguerra, A. Olivas, S. Fuentes, D. Galvan, M. J. Yacaman, *J. Catal.* **2005**, *234*, 182–190.
[5] P.-Y. Prodhomme, P. Raybaud, H. Toulhoat, *J. Catal.* **2011**, *280*, 178–195.
[6] J. Hu, B. Huang, C. Zhang, Z. Wang, Y. An, D. Zhou, H. Lin, M. K. H. Leung, S. Yang, *Energy Environ. Sci.* **2017**, *10*, 593–603.
[7] H. G. S. Casalongue, J. D. Benck, C. Tsai, R. K. B. Karlsson, S. Kaya, M. L. Ng, L. G. M. Pettersson, F. Abild-Pedersen, J. K. Nørskov, H. Ogasawara, et al., *J. Phys. Chem. C* **2014**, *118*, 29252–29259.
[8] R. Canton-Vitoria, Y. Sayed-Ahmad-Baraza, M. Pelaez-Fernandez, R. Arenal, C. Bittencourt, C. P. Ewels, N. Tagmatarchis, *Npj 2D Mater. Appl.* **2017**, *1*, DOI 10.1038/s41699-017-0012-8.
[9] S. Bertolazzi, M. Gobbi, Y. Zhao, C. Backes, P. Samorì, *Chem. Soc. Rev.* **2018**, *47*, 6845–6888.
[10] N. M. Galea, E. S. Kadantsev, T. Ziegler, *J. Phys. Chem. C* **2009**, *113*, 193–203.
[11] Y. Li, D. Wu, Z. Zhou, C. R. Cabrera, Z. Chen, *J. Phys. Chem. Lett.* **2012**, *3*, 2221–2227.
[12] Z. Wang, H. Li, Z. Liu, Z. Shi, J. Lu, K. Suenaga, S.-K. Joung, T. Okazaki, Z. Gu, J. Zhou, et al., *J. Am. Chem. Soc.* **2010**, *132*, 13840–13847.
[13] H. Schweiger, P. Raybaud, G. Kresse, H. Toulhoat, *J. Catal.* **2002**, *207*, 76–87.
[14] D. Cao, T. Shen, P. Liang, X. Chen, H. Shu, *J. Phys. Chem. C* **2015**, *119*, 4294–4301.
[15] H. G. Füchtbauer, A. K. Tuxen, Z. Li, H. Topsøe, J. V. Lauritsen, F. Besenbacher, *Top. Catal.* **2014**, *57*, 207–214.
[16] J. V. Lauritsen, J. Kibsgaard, S. Helveg, H. Topsøe, B. S. Clausen, E. Lægsgaard, F. Besenbacher, *Nat. Nanotechnol.* **2007**, *2*, 53–58.
[17] S. Yu, W. Zheng, *Phys Chem Chem Phys* **2016**, *18*, 4675–4683.
[18] R. J. Wu, M. L. Odlyzko, K. A. Mkhoyan, *Ultramicroscopy* **2014**, *147*, 8–20.
[19] M. V. Bollinger, K. W. Jacobsen, J. K. Nørskov, *Phys. Rev. B* **2003**, *67*, DOI 10.1103/PhysRevB.67.085410.
[20] L. S. Byskov, J. K. Nørskov, B. S. Clausen, H. Topsøe, *J. Catal.* **1999**, *187*, 109–122.
[21] M. C. Lucking, J. Bang, H. Terrones, Y.-Y. Sun, S. Zhang, *Chem. Mater.* **2015**, *27*, 3326–3331.
[22] J. V. Lauritsen, M. V. Bollinger, E. Lægsgaard, K. W. Jacobsen, J. K. Nørskov, B. S. Clausen, H. Topsøe, F. Besenbacher, *J. Catal.* **2004**, *221*, 510–522.
[23] S. Helveg, J. V. Lauritsen, E. L\a egsgaard, I. Stensgaard, J. K. Nørskov, B. S. Clausen, H. Topsøe, F. Besenbacher, *Phys. Rev. Lett.* **2000**, *84*, 951.
[24] S. S. Grønborg, N. Salazar, A. Bruix, J. Rodríguez-Fernández, S. D. Thomsen, B. Hammer, J. V. Lauritsen, *Nat. Commun.* **2018**, *9*, 2211.
[25] B. Hinnemann, J. K. Nørskov, H. Topsøe, *J. Phys. Chem. B* **2005**, *109*, 2245–2253.
[26] S. Cristol, J. F. Paul, E. Payen, D. Bougeard, S. Clémendot, F.

Hutschka, *J. Phys. Chem. B* **2000**, *104*, 11220–11229.
[27] L. F. Seivane, H. Barron, S. Botti, M. A. L. Marques, Á. Rubio, X. López-Lozano, *J. Mater. Res.* **2013**, *28*, 240–249.
[28] H. Vahrenkamp, *Angew. Chem. Int. Ed. Engl.* **1975**, *14*, 322–329.
[29] C. G. Young, *J. Inorg. Biochem.* **2007**, *101*, 1562–1585.
[30] N. Dou, B. Peng, Q. Li, Q. Luo, Y. Xie, R. B. King, H. F. Schaefer, *Polyhedron* **2013**, *52*, 1375–1384.
[31] M. Rakowski DuBois, D. L. DuBois, M. C. VanDerveer, R. C. Haltiwanger, *Inorg. Chem.* **1981**, *20*, 3064–3071.
[32] A. Müller, W. Eltzner, N. Mohan, *Angew. Chem. Int. Ed. Engl.* **1979**, *18*, 168–169.
[33] C. Giannotti, A. M. Ducourant, H. Chanaud, A. Chiaroni, D. Riche, *J. Organomet. Chem.* **1977**, *140*, 289–295.
[34] F. Sécheresse, J. Lefebvre, J. C. Daran, Y. Jeannin, *Inorganica Chim. Acta* **1981**, *54*, L175–L176.
[35] W. A. Herrmann, J. Rohrmann, A. Schäfer, *J. Organomet. Chem.* **1984**, *265*, c1–c5.
[36] L. Yoong. Goh, T. W. Hambley, G. B. Robertson, *Organometallics* **1987**, *6*, 1051–1057.
[37] W. B. Jensen, *J. Chem. Educ.* **2005**, *82*, 28.
[38] P. D. Fleischauer, J. R. Lince, P. A. Bertrand, R. Bauer, *Langmuir* **1989**, *5*, 1009–1015.
[39] R. Hoffmann, J. M. Howell, A. R. Rossi, *J. Am. Chem. Soc.* **1976**, *98*, 2484–2492.
[40] M. H. Whangbo, E. Canadell, *J. Am. Chem. Soc.* **1992**, *114*, 9587–9600.
[41] C. Rovira, M. H. Whangbo, *Inorg. Chem.* **1993**, *32*, 4094–4097.
[42] J. K. Burdett, T. Hughbanks, *Inorg. Chem.* **1985**, *24*, 1741–1750.
[43] R. Jones, P. R. Briddon, in *Identif. Defects Semicond.*, Academic Press, Boston, **1998**.
[44] M. J. Rayson, P. R. Briddon, *Phys. Rev. B* **2009**, *80*, DOI 10.1103/PhysRevB.80.205104.
[45] P. R. Briddon, M. J. Rayson, *Phys. Status Solidi B* **2011**, *248*, 1309–1318.
[46] P. r. Briddon, R. Jones, *Phys. Status Solidi B* **2000**, *217*, 131–171.
[47] C. Hartwigsen, S. Gø edecker, J. Hutter, *Phys. Rev. B* **1998**, *58*, 3641.

Entry for the Table of Contents

FULL PAPER

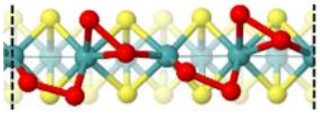

Mo-100%S

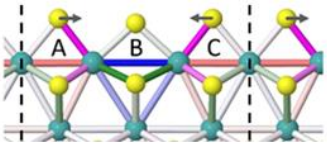

Mo-50%S

A complete density functional study of S-terminated edges in 1H-MoS_2 finds new potential entropically favoured structures for Mo-100%S edges, and proposes a Peierl's distortion model explaining the stability of triply periodic Mo-50%S edges.

*Yuman Sayed-Ahmad-Baraza, Christopher P. Ewels**

Page No. – Page No.

Stability, structure and reconstruction of 1H-edges in MoS_2